JACS JOURNAL OF THE AMERICAN CHEMICAL SOCIETY

Article

Cite This: J. Am. Chem. Soc. 2020, 142, 552−563

pubs.acs.org/JACS

Ligand Redox Noninnocence in [Co^{III}(TAML)]$^{0/-}$ Complexes Affects Nitrene Formation

Nicolaas P. van Leest,[†] Martijn A. Tepaske,[†] Jean-Pierre H. Oudsen,[‡] Bas Venderbosch,[‡] Niels R. Rietdijk,[†] Maxime A. Siegler,[§] Moniek Tromp,[‡] Jarl Ivar van der Vlugt,*[,†] and Bas de Bruin*[,†]

[†]Homogeneous, Supramolecular and Bio-Inspired Catalysis Group and [‡]Sustainable Materials Characterization Group, van't Hoff Institute for Molecular Sciences (HIMS), University of Amsterdam, Science Park 904, 1098XH Amsterdam, The Netherlands

[§]Department of Chemistry, Johns Hopkins University, Baltimore, Maryland 21218, United States

Supporting Information

ABSTRACT: The redox noninnocence of the TAML scaffold in cobalt-TAML (tetra-amido macrocyclic ligand) complexes has been under debate since 2006. In this work, we demonstrate with a variety of spectroscopic measurements that the TAML backbone in the anionic complex [**Co^{III}(TAML^{red})**]$^-$ is truly redox noninnocent and that one-electron oxidation affords [**Co^{III}(TAML^{sq})**]. Multireference (CASSCF) calculations show that the electronic structure of [**Co^{III}(TAML^{sq})**] is best described as an intermediate spin (S = 1) cobalt(III) center that is antiferromagnetically coupled to a ligand-centered radical, affording an overall doublet (S = $^1/_2$) ground-state. Reaction of the cobalt(III)-TAML complexes with PhINNs as a nitrene precursor leads to TAML-centered oxidation and produces nitrene radical complexes without oxidation of the metal ion. The ligand redox state (TAML^{red} or TAML^{sq}) determines whether mono- or bis-nitrene radical complexes are formed. Reaction of [**Co^{III}(TAML^{sq})**] or [**Co^{III}(TAML^{red})**]$^-$ with PhINNs results in the formation of [**Co^{III}(TAML^{q})(N$^{\bullet}$Ns)**] and [**Co^{III}(TAML^{q})(N$^{\bullet}$Ns)$_2$**]$^-$, respectively. Herein, ligand-to-substrate single-electron transfer results in one-electron-reduced Fischer-type nitrene radicals (N$^{\bullet}$Ns$^-$) that are intermediates in catalytic nitrene transfer to styrene. These nitrene radical species were characterized by EPR, XANES, and UV−vis spectroscopy, high-resolution mass spectrometry, magnetic moment measurements, and supporting CASSCF calculations.

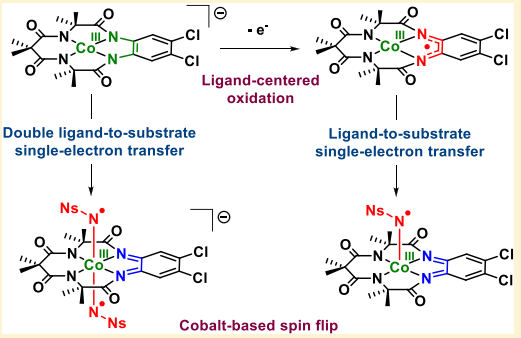

INTRODUCTION

The use of base metals and redox noninnocent (or redox-active) ligands in radical-type carbene, oxo, and nitrene transfer reactions has evolved as a powerful tool for the direct functionalization of (unactivated) C−H bonds and olefins.[1] The functionalized products of these reactions are motifs in pharmaceuticals and agrochemicals and are therefore highly valued.[2] N-group transfer reactivity is an efficient way to afford the direct synthesis of secondary amines and aziridines, of which the synthesis otherwise typically requires harsh reaction conditions or multiple steps.[3] Generation of the essential catalytic metal-nitrene intermediates has been achieved with second- and third-row transition metals (Ru,[4] Rh,[5] Pd,[6] Ag[7], and Au[8]) as well as more abundant base metals (Mn,[9] Fe,[10] Co,[11] Ni[12], and Cu[13]).

Our group, in collaboration with the Zhang group, has studied the formation and reactivity of nitrene adducts of cobalt(II)-porphyrin complexes, which are competent catalysts for a range of (enantioselective) amination and aziridination reactions.[11a,d−j,14] The mononitrene species generated on cobalt upon reaction with an organic azide is most accurately described as a one-electron-reduced Fischer-type nitrene radical.[14b] This interesting electronic structure is the result of metal-to-substrate single-electron transfer (SET), wherein cobalt is oxidized from Co^{II} to Co^{III} and the nitrene is reduced by one electron to produce a nitrene radical (N$^{\bullet}$R$^-$) complex with single-electron population of the π symmetric Co−N antibonding orbital. Interestingly, the reaction of cobalt(II)-porphyrins with iminoiodinanes (PhINNs, Ns = nosyl) led to the formation of bis-nitrene radical species with two one-electron-reduced Fischer-type nitrenes, wherein the second nitrene is reduced via ligand-to-substrate SET. Intrigued by these nitrene-transfer catalysts, we became interested in the possibility of nitrene radical formation on square planar cobalt(III) platforms involving solely ligand-to-substrate single-electron transfer[15] by studying systems containing redox-active ligands for which metal-to-substrate SET is difficult or even impossible.

When searching for suitable redox-active macrocyclic tetradentate ligand platforms that enforce a square planar coordination geometry around cobalt in an oxidation state higher than +II, we decided to investigate the tetra-amido

Received: October 30, 2019
Published: December 17, 2019

DOI: 10.1021/jacs.9b11715
J. Am. Chem. Soc. 2020, 142, 552−563

macrocyclic ligand (TAML) platform designed by Collins' group.[16] The general structure of a TAML that met the aforementioned requirements is depicted in Scheme 1. More-

Scheme 1. General Structure of the TAML Scaffold and the Potential Redox Noninnocence of the Backbone[a]

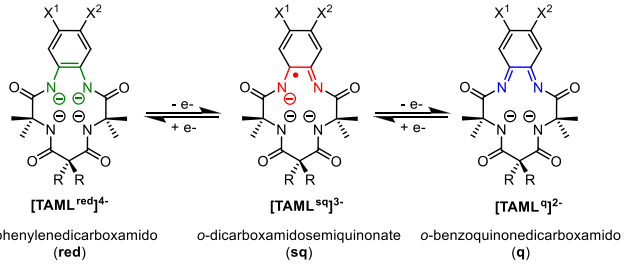

[a] X^1 = Cl, H, NO_2, OMe. X^2 = Cl, H. R = Et, Me, F.[16]

over, the potential redox noninnocence of TAML and related *o*-phenylenedicarboxamido complexes has been proposed in the literature, and for clarity, we will follow the nomenclature as presented in Scheme 1 for the fully reduced tetra-anion (red), mono-oxidized trianionic ligand-centered radical (sq), and fully oxidized dianion (q).[16,17]

Iron complexes of these TAML activators have found widespread use in oxidation chemistry, and TAML complexes with Cr, Mn, Fe, Co, Ni and Cu have been reported with many variations of the TAML scaffold.[16,18] Interestingly, ligand-centered oxidation of an $[Fe^{V}(TAML^{red})(NTs)]^{-}$ complex was shown to afford $[Fe^{V}(TAML^{sq})(NTs)]$, which is a more active nitrene transfer species toward activated C–H bonds (bond dissociation energy between 75 and 80 kcal mol^{-1}) and thioanisole than the reduced analogue.[19] A similar trend was observed for a manganese-imido complex, wherein $[Mn^{V}(TAML^{red})(NMes)]^{-}$ (Mes = mesityl) proved to be unreactive and metal-centered oxidized complex $[Mn^{VI}(TAML^{red})(NMes)]$ could be used for hydrogen atom transfer reactions and nitrene transfer to thioanisole.[20]

Apparently, the redox activity of the TAML ligand varies from complex to complex, depending on the metal and other ligands, and both metal- and ligand-centered redox processes can be used to influence the nitrene-transfer reactivity.

Specific $[Co^{III}(TAML^{red})]^{-}$ complexes[21] have been used for electrochemical water oxidation[22,23] and oxygen reduction,[24] cycloaddition of CO_2 to epoxides,[25] electrochemical sensing of H_2O_2,[26] oxo transfer to C–H bonds,[27] and electron-transfer reactions.[28] However, to the best of our knowledge, no nitrene transfer reactions or stoichiometric reactions leading to the formation of Co(TAML)-based imido- or nitrene-complexes have been reported to date. Moreover, contrary to chemistry with iron, the existence of TAML-centered redox processes in cobalt complexes is still under debate (Figure 1).

Collins et al.[21] reported the synthesis and characterization of an anionic $[Co^{III}(TAML^{red})]^{-}$ complex with a diamidophenyl backbone in 1991. The anionic parent complex was characterized as a triplet with an $S = 1$ Co center and a fully reduced *o*-phenylenedicarboxamido ligand. The oxidation of this complex afforded a neutral $S = {}^{1}/_{2}$ system for which crystallographic bond metrics indicated single-electron oxidation of the ligand and electron paramagnetic resonance (EPR) data hinted at a cobalt-centered radical (Figure 1). This data was interpreted in 1998 as corresponding to an $S = 1$ cobalt(III) center antiferromagnetically coupled to a ligand-centered radical ($[Co^{III}(TAML^{sq})]$).[28] Ghosh et al.[29] reported an elaborate density functional theory (DFT) study on the ligand noninnocence of multiple variations of the TAML backbone and suggested that the electronic structure of $[Co^{III}(TAML^{sq})]$ is better described as $[Co^{IV}(TAML^{red})]$ (Figure 1). Their assignment was based on the Mulliken spin density, which was solely localized on cobalt. Collins and co-workers[18] critically reinterpreted these spin densities as being evidence of an $S = 1$ Co^{III} center. It should be noted that multireference post-Hartree–Fock methods were not accessible at the time, and possible broken-symmetry solutions were apparently not explored. As such, optional antiferromagnetic coupling between an $S = 1$ Co center and a ligand-centered

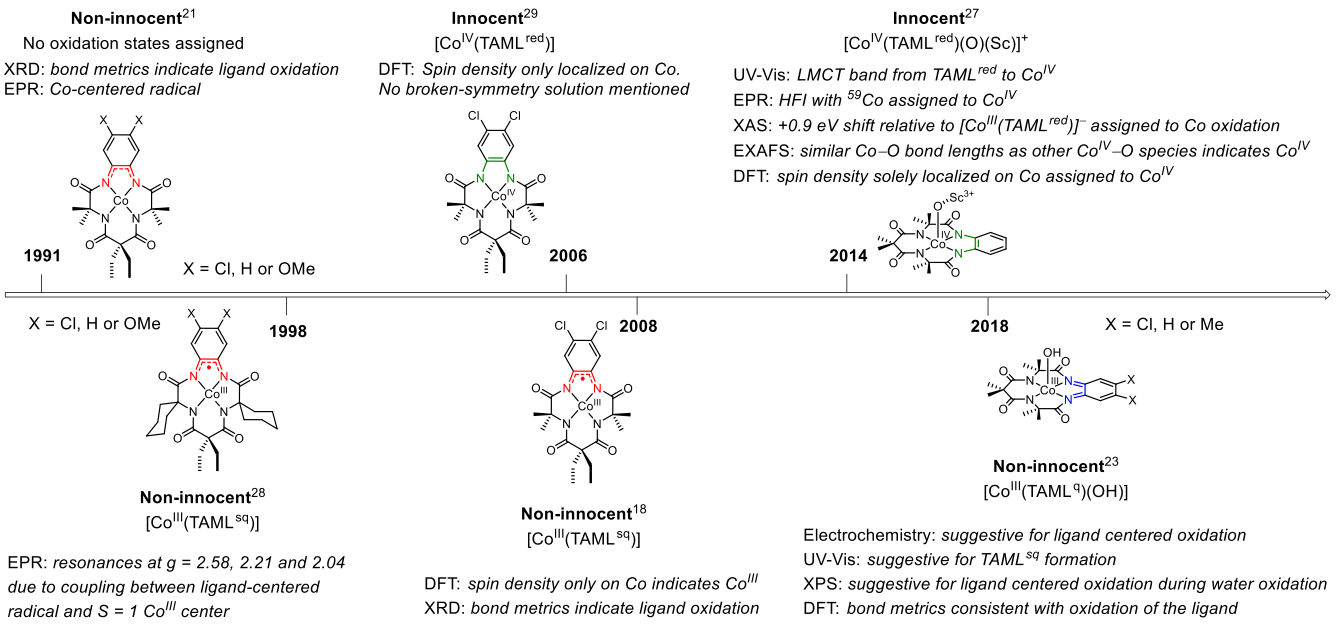

Figure 1. Interpretation of the ligand (non)innocence in cobalt-TAML complexes in chronological order. HFI = hyperfine interaction.

DOI: 10.1021/jacs.9b11715
J. Am. Chem. Soc. 2020, 142, 552–563

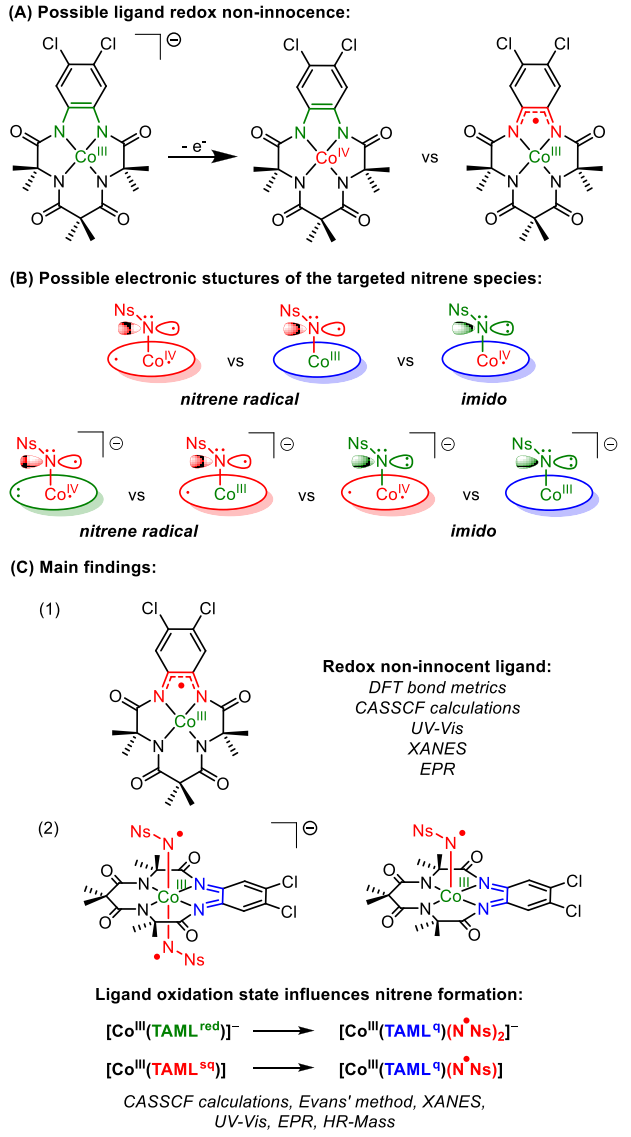

Figure 2. (A) Electronic structure questions regarding the redox noninnocence of the TAML scaffold. (B) Possible electronic structures of the targeted nitrene species. The ligand color coding is as presented in Scheme 1. (C) Main findings with the assignment of the TAML scaffold being redox noninnocent in the coordination sphere of cobalt and its influence on nitrene (radical) formation.

radical could have remained hidden in the applied DFT calculations.

Innocent behavior of the TAML scaffold was claimed in an electrochemical study reported in 2014[30] as well as in the characterization of Lewis acid-stabilized oxo-complex [Co^{IV}(TAML^{red})(O)].[27] The TAML^{red} and Co^{IV} oxidation states in an Sc^{3+}-bound [Co^{IV}(TAML^{red})(O)]$^{2-}$ complex were based on UV−vis, EPR, XANES (X-ray absorption near edge spectroscopy), and EXAFS (extended X-ray absorption fine structure) studies, in combination with DFT-calculated Mulliken spin densities.[27] On the contrary, TAML-centered redox activity in [Co^{III}(TAML^{q})(OH)] was claimed in 2018 on the basis of UV−vis, EPR, and XPS (X-ray photoelectron spectroscopy) studies.[23]

Given (i) the contrasting descriptions of ligand and cobalt oxidation states in [Co(TAML)] complexes, (ii) our interest in generating cobalt-nitrene radical intermediates via ligand-to-substrate SET, and (iii) the previous characterization of [Fe(TAML)(imido)], [Mn(TAML)(imido)], and [Co(TAML)(oxo)] complexes, we set out to answer the following research questions:

Is the ligand in [Co(TAML)] complexes redox noninnocent, and can the different assignments in the literature be reconciled? (See Figure 2A.)

Can the [Co(TAML)] platform be used to generate (catalytically competent) cobalt-nitrene (radical) species, and what is the influence of the (ligand) oxidation state on the (electronic) structure of the targeted nitrene (radical) species? (See Figure 2B.)

In case the TAML ligand platform is indeed redox-active, can we use this feature for ligand-to-substrate SET to produce nitrene radical species at square planar cobalt(III) species? (See Figure 2B).

The main findings of the investigations presented in this article are summarized in Figure 2C.

RESULTS AND DISCUSSION

Ligand-Centered Oxidation of [Co^{III}(TAML^{red})]$^{-}$. The parent [Co^{III}(TAML^{red})]$^{-}$ complex was obtained according to an adapted literature procedure.[21,31] After a five-step synthesis procedure to obtain the ligand (**TAMLH$_4$**), coordination of Co^{II} to the fully deprotonated ligand (generated using *n*-BuLi) and aerobic oxidation afforded **Li[Co^{III}(TAML^{red})]** or **PPh$_4$[Co^{III}(TAML^{red})]** after salt metathesis with PPh$_4$Cl (Scheme 2). Crystals suitable for singe crystal X-ray diffraction

Scheme 2. (A) Formation of Li[Co^{III}(TAML^{red})] and PPh$_4$[Co^{III}(TAML^{red})] from TAMLH$_4$, with Thermal Displacement Ellipsoid Plots (50% Probability Level) of TAMLH$_4$ (B) and PPh$_4$[Co^{III}(TAML^{red})] (C). H Atoms (Except for NH) and Lattice Solvent (THF for PPh$_4$[Co^{III}(TAML^{red})]) Removed for Clarity

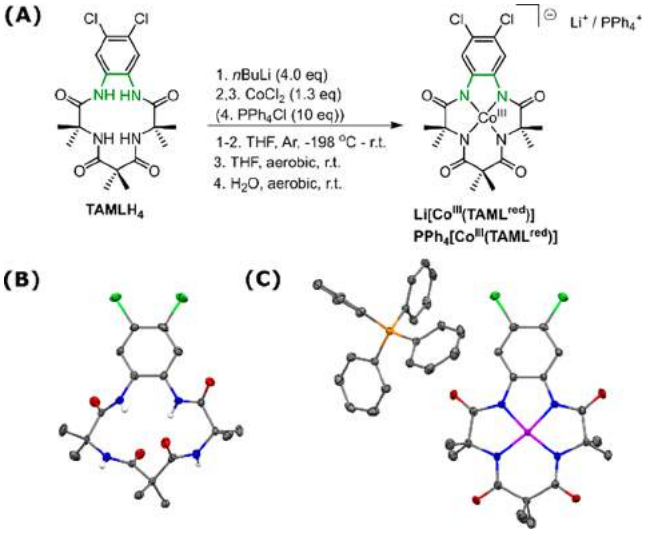

(XRD) analysis of **TAMLH$_4$** and **PPh$_4$[Co^{III}(TAML^{red})]** were grown by the vapor diffusion of pentane into concentrated THF solutions of the ligand or complex, respectively. The solid state structure of **PPh$_4$[Co^{III}(TAML^{red})]** displays a square planar geometry around cobalt and a noncoordinating THF molecule in the crystal lattice. As expected and in accordance with the literature,[21] an analysis of the crystallographic bond metrics (Supporting Information) of the diamidophenyl ring in

DOI: 10.1021/jacs.9b11715
J. Am. Chem. Soc. 2020, 142, 552−563

TAMLH$_4$ and **PPh$_4$[Co^{III}(TAML^{red})]** supports the preservation of aromaticity upon coordination to cobalt, with the ligand being fully reduced ((**TAML^{red}**)$^{4-}$) and the metal adopting the Co^{III} oxidation state. The effective magnetic moment of **PPh$_4$[Co^{III}(TAML^{red})]**, as determined via the Evans' method,[32] indicated a triplet ($S = 1$) ground state ($\mu_{eff} = 2.94\mu_B$). This is in accordance with the literature and is expected for an intermediate-spin Co^{III} center with two parallel metal-centered unpaired electrons.[21] The DFT-optimized structure of [**Co^{III}(TAML^{red})**]$^-$ in the triplet state at the BP86/def2-TZVP level of theory is consistent with these observations, and the calculated bond metrics closely match the experimental bond lengths (SI).

The electrochemical oxidation of **PPh$_4$[Co^{III}(TAML^{red})]** in CH_2Cl_2 (Scheme 3A) using cyclic voltammetry displays three

Scheme 3. (A) Cyclic Voltammogram of PPh$_4$[Co^{III}(TAML^{red})] in DCM (Details in the SI), (B) UV−vis−SEC Oxidation of PPh$_4$[Co^{III}(TAML^{red})] in DCM (Details in the SI), (C) Oxidation of [Co^{III}(TAML^{red})]$^-$ to [Co^{III}(TAML^{sq})] with (Thi)BF$_4$, and (D) UV−vis Titration of PPh$_4$[Co^{III}(TAML^{red})] in DCM (0.15 mM) with Increasing Amounts of (Thi)BF$_4$

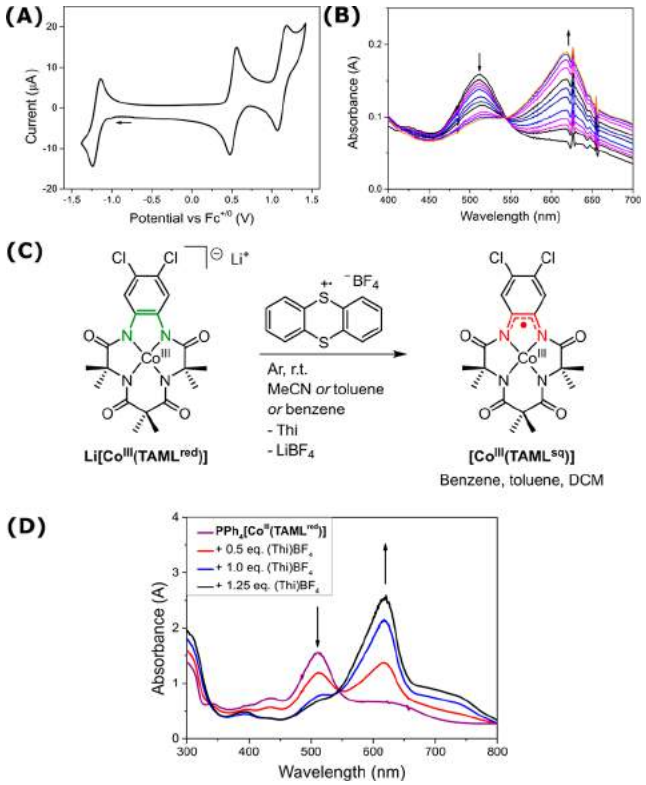

fully reversible redox events at $E^{1}/_{2} = -1.18$, +0.53, and +1.13 V vs Fc$^{+/0}$, which are attributed to metal-centered reduction (Co$^{III/II}$) and two ligand-centered oxidations (TAML$^{red/sq}$ and TAML$^{sq/q}$) respectively (vide infra).[33] UV−vis spectroelectrochemical (UV−vis−SEC) monitoring of the oxidation event at +0.53 V vs Fc$^{+/0}$ shows the disappearance of **PPh$_4$[Co^{III}(TAML^{red})]** ($\lambda_{max} = 510$ nm) and the concomitant appearance of the characteristic absorption band of [**Co^{III}(TAML^{sq})**] ($\lambda_{max} = 623$ nm) with an isosbestic point at 545 nm (Scheme 3B).[21,23,34,35] For clarity we already assigned the electronic structure of [**Co^{III}(TAML^{sq})**] in the following descriptions. In the following sections we will further elaborate on the measurements and calculations leading to this assignment.

Chemical oxidation of TAML complexes with ceric ammonium nitrate ($(NH_4)_2[Ce(NO_3)_6]$) typically requires excess oxidant and large volumes of solvent to extract the product.[21] For purple-colored **PPh$_4$[Co^{III}(TAML^{red})]** and **Li[Co^{III}(TAML^{red})]**, oxidation with a stoichiometric amount of thianthrenium tetrafluoroborate ((Thi)BF$_4$) ($E^{o_1}/_2 = 0.86$ V vs Fc$^{+/0}$)[36] cleanly afforded the blue-colored [**Co^{III}(TAML^{sq})**] complex (Scheme 3C). A UV−vis titration gave data identical to that obtained from UV−vis−SEC monitoring of the oxidation event at +0.53 V vs Fc$^{+/0}$ (Scheme 3D).

The effective magnetic moment of [**Co^{III}(TAML^{sq})**] ($\mu_{eff} = 1.88\mu_B$, Evans' method) was found to be consistent with an overall net doublet ($S = {}^1/_2$) ground state. Room-temperature (r.t.) X-band EPR studies in CH_2Cl_2 or toluene reveal a signal characteristic of a net $S = {}^1/_2$ system with unpaired electron density on cobalt ($g_{iso} = 2.22$) (Figure 3A). EPR measurements

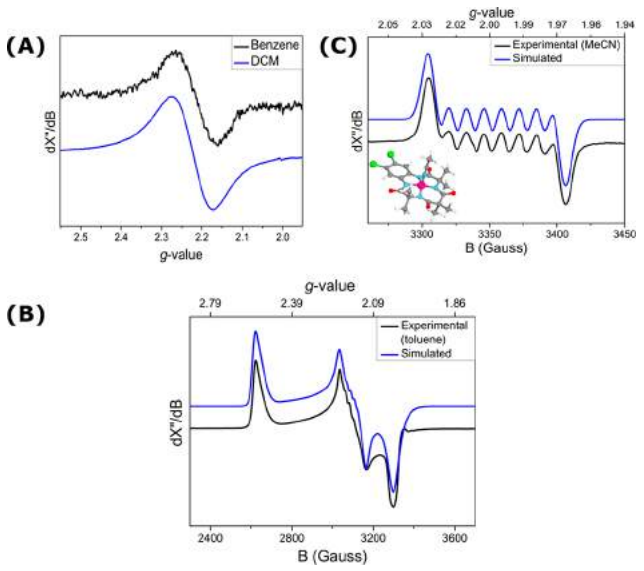

Figure 3. (A) X-band EPR spectrum of [**Co^{III}(TAML^{sq})**] in benzene at r.t. (black line: microwave freq. 9.390167 GHz, mod. amp. 4 G, and power 2.518 mW) and CH_2Cl_2 (blue line: microwave freq. 9.3966 GHz, mod. amp. 5 G, and power 2.000 mW) with $g_{iso} = 2.22$. (B) Experimental (black) and simulated (blue) X-band EPR spectrum of [**Co^{III}(TAML^{sq})**] in toluene at 10 K. Microwave freq. 9.365984 GHz, mod. amp. 4 G, and power 2.000 mW. Simulation parameters: $g_x = 2.03$, $g_y = 2.16$, $g_z = 2.54$, $A^{Co}{}_x = 5.0$ MHz, $A^{Co}{}_y = 50.0$ MHz, $A^{Co}{}_z = 20.0$ MHz, linear A strain −0.018 (z direction), and quadratic A strain −18 (x direction) and −2 (y direction). (C) Experimental (black) and simulated (blue) X-band EPR spectra of [**Co^{III}(TAML^{sq})(MeCN)**] at r.t. in MeCN and the DFT (BP86/def2-TZVP/disp3)-optimized structure. Microwave freq. 9.3886 GHz, mod. amp. 3 G, and power 0.7962 mW. Simulated (calculated; B3LYP/def2-TZVP)) parameters: $g_{iso} = 2.00$ (2.00) and $A^{Co}{}_{iso} = 36.0$ (34.2) MHz.

at 10 K in toluene glass showed a rhombic signal with $g_x = 2.03$, $g_y = 2.16$, $g_z = 2.54$, and partially unresolved cobalt hyperfine interactions (HFIs) (Figure 3B). The inclusion of ^{59}Co ($I = 7/2$ nucleus) HFIs ($A^{Co}{}_x = 5.0$ MHz, $A^{Co}{}_y = 50.0$ MHz, $A^{Co}{}_z = 20.0$ MHz) is necessary for an accurate simulation of the spectrum. The DFT-calculated cobalt HFIs are overestimated (B3LYP/def2-TZVP: $g_x = 2.04$, $g_y = 2.25$, $g_z = 2.26$, $A^{Co}{}_x = 166.3$ MHz, $A^{Co}{}_y = 199.8$ MHz, and $A^{Co}{}_z = 641.3$ MHz), which we attribute

DOI: 10.1021/jacs.9b11715
J. Am. Chem. Soc. 2020, 142, 552−563

to the erroneous description of multireference systems with DFT methods (vide infra). Interestingly, the isotropic X-band EPR spectrum measured in MeCN (Figure 3C) revealed an eight-line pattern at g_{iso} = 2.00 attributed to hyperfine coupling with cobalt (A^{Co}_{iso} = 36.0 MHz) in [**Co^{III}(TAML^{sq})(MeCN)**], which is in excellent agreement with the DFT-calculated parameters (B3LYP/def2-TZVP: g_{iso} = 2.00, A^{Co}_{iso} = 34.2 MHz). Notably, this species has a single-reference doublet electronic structure with the unpaired electron residing in a cobalt-ligand π* orbital (strongly delocalized over cobalt and the ligand; see the SI).

The cobalt oxidation state of the four-coordinate complexes was further investigated using Co K-edge X-ray absorption near edge spectroscopy analysis. The Co K-edge XANES spectra of **PPh$_4$[Co^{III}(TAML^{red})]** and [**Co^{III}(TAML^{sq})**] in toluene are compared in Figure 4. The edge position was 7721 eV for both

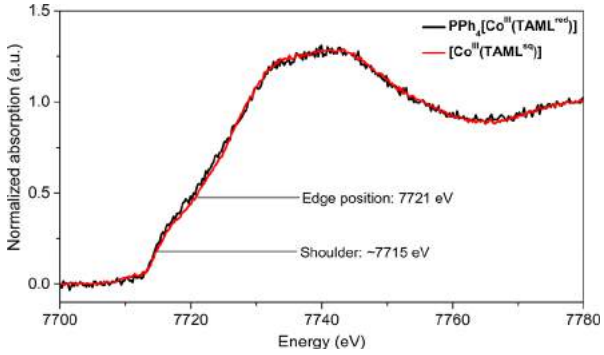

Figure 4. Co K-edge XANES analysis of **PPh$_4$[Co^{III}(TAML^{red})]** (black) and [**Co^{III}(TAML^{sq})**] (red) in toluene.

complexes. Both spectra are identical, which is in line with the same oxidation state (+III) and similar coordination geometry of cobalt in the two complexes. The +III oxidation state of cobalt was already found in **PPh$_4$[Co^{III}(TAML^{red})]** (according to XRD-derived bond metric analysis, vide supra), and the observed edge position is equal to a related [Co^{III}(TAML)]$^-$ complex.[27] The shoulder at approximately 7715 eV in the Co K-edge XANES spectra is typical for square planar Co complexes, including square planar Co-porphyrin complexes and a related cobalt-TAML complex.[14b,27] The main edge feature arises primarily from 1s → 4p electron transitions, whereas the feature at 7715 eV is commonly assigned to 1s → 4p$_z$ and ligand-to-metal charge transfer (LMCT) shakedown transitions.[37]

In agreement with previous studies,[27,29] DFT calculations with various GGA and hybrid functionals (BP86, B3LYP, PBE, and OPBE; see the SI for details) gave unsatisfactory results for the Co(TAML)-type complexes under investigation. An illustrative example of the problem encountered with DFT is found in the challenging description of the net-doublet ground state of the [**Co^{III}(TAML^{sq})**] complex. Distinguishing between a genuine Co^{IV} complex and a multireference electronic structure solution involving antiferromagnetic coupling between an S = 1 Co^{III} center and a TAML ligand-centered radical (as indicated by the B3LYP broken-symmetry DFT solution) is very difficult, if not impossible, when relying only on single-reference computational methods (such as DFT).[38] We therefore decided to turn to multireference N-electron valence state perturbation theory (NEVPT2)-corrected complete active space self consistent field (CASSCF) calculations for a proper description of the electronic structures of the Co(TAML)-type complexes described in this article.[39]

CASSCF calculations were initiated on the anionic [**Co^{III}(TAML^{red})**]$^-$ complex by the inclusion of all cobalt d orbitals and those ligand π orbitals (L$_\pi$) that could have an interaction with cobalt. In the final CASSCF(14,13) calculation, all initial orbitals were preserved in the active space, except for the d$_{xy}$ orbital, which is uncorrelated (occupancy of 2.00).[40] A selection of the most relevant active orbitals with their occupancies (in parentheses) is given in Figure 5A. Löwdin

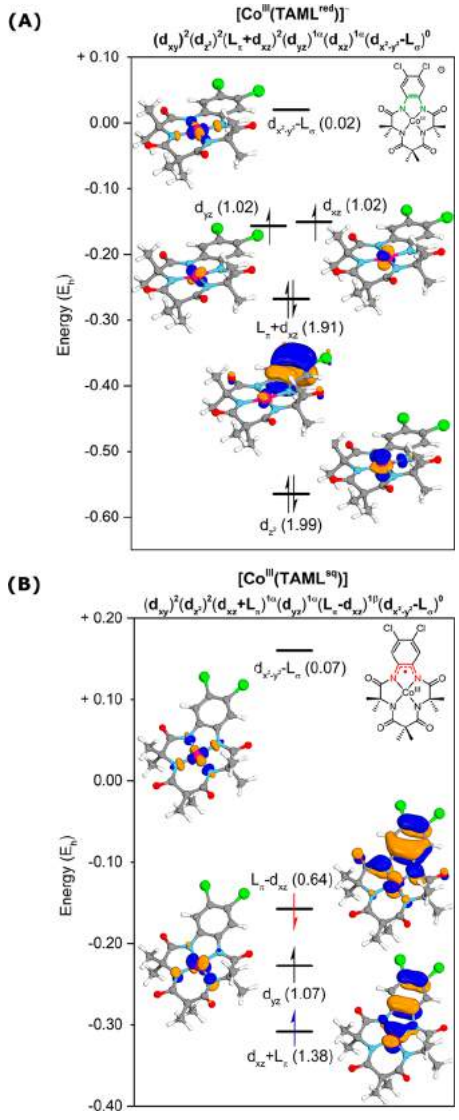

Figure 5. Relevant active orbitals and occupancies (in parentheses) of NEVPT2-corrected CASSCF(14,13) on [**Co^{III}(TAML^{red})**]$^-$ (A) and CASSCF(13,12) on [**Co^{III}(TAML^{sq})**] (B).

population analysis of the electronic configuration of the d shell gave $(d_{xy})^{2.00}(d_{z^2})^{1.99}(d_{yz})^{1.02}(d_{xz})^{1.02}$, consistent with the assigned +III oxidation state of cobalt. Notably, the L$_\pi$ orbital at $-0.268E_h$ has a weak bonding interaction with the d$_{xz}$ orbital and is fully filled (occupancy 1.91), consistent with the fully reduced oxidation state of the ligand.

CASSCF(13,12) calculations on the neutral [**Co^{III}(TAML^{sq})**] complex included a similar active space as for the parent anionic complex and revealed substantial

DOI: 10.1021/jacs.9b11715
J. Am. Chem. Soc. 2020, 142, 552−563

multireference character. The uncorrelated d_{z^2} and d_{xy} orbitals (occupancy 2.00) were not preserved in the active space.[40] The reduced charge on the complex causes increased stabilization of the cobalt d orbitals compared to the parent anionic complex, which increases overlap between the d_{xz} and L_π orbitals (Figure 5B). Because of this stabilization, the bonding and antibonding combinations of the d_{xz} and L_π orbitals are composed of substantial contributions from both d_{xz} and L_π. As a result of three orbitals being close in energy, significant population of the $L_\pi - d_{xz}$ antibonding combination (occupancy 0.64) from the $d_{xz} + L_\pi$ bonding combination (occupancy 1.38) occurs, while the d_{yz} orbital is singly occupied (1.07). The net-doublet ground state of the neutral $[\mathbf{Co^{III}(TAML^{sq})}]$ complex is thus best described as an $S = 1$ Co^{III} center that is antiferromagnetically coupled to an $S = {}^1/_2$ TAML-centered radical, leading to a net-doublet system with a $(d_{xy})^{2.00}(d_{z^2})^{2.00}(d_{xz} + L_\pi)^{1.38}(d_{yz})^{1.07}(L_\pi - d_{xz})^{0.64}$ electronic structure, in agreement with the early interpretation of Collins.[28] Excitation energies derived from the CASSCF(13, 12) calculations revealed that the absorption band observed at λ_{max} = 623 nm (Scheme 3B,D) is indeed characteristic of the ligand-centered radical. The corresponding calculated excitation (at 625 nm) is composed of ligand-centered $L_\pi \rightarrow L_\pi - d_{xz}$ and metal-to-ligand ($d_{xz} + L_\pi \rightarrow L_\pi - d_{xz}$ and $d_{yz} \rightarrow L_\pi - d_{xz}$) charge-transfer processes, with the ligand-centered radical orbital being the acceptor in all cases.

The combined data from magnetic moment measurements, EPR, UV−vis, and XANES spectroscopy, and NEVPT2-CASSCF calculations reveal that the oxidation of $[\mathbf{Co^{III}(TAML^{red})}]^-$ is ligand-centered, giving rise to the formation of $[\mathbf{Co^{III}(TAML^{sq})}]$, wherein cobalt retains its +III oxidation state and its square planar coordination geometry.

Synthesis of $[\mathbf{Co^{III}(TAML^{q})(NNs)_2}]^-$ and $[\mathbf{Co^{III}(TAML^{q})(NNs)}]$ via Ligand-to-Substrate SET. With a proper understanding of their electronic structure, confirming that both complexes are square planar cobalt(III) species featuring a redox-active ligand but are in two different ligand oxidation states, we next set out to investigate nitrene formation at the anionic $[\mathbf{Co^{III}(TAML^{red})}]^-$ and neutral $[\mathbf{Co^{III}(TAML^{sq})}]$ complexes. We were particularly interested in exploring the influence of the ligand oxidation state on the structure and overall composition of the targeted nitrene adducts.

The addition of 1 equiv of the nitrene precursor PhINNs to $\mathbf{PPh_4[Co^{III}(TAML^{red})]}$ in CH_2Cl_2 at r.t. led to a mixture of starting material, mononitrene adduct $[\mathbf{Co(TAML)(NNs)}]^-$, and trace amounts of bis-nitrene adduct $[\mathbf{Co(TAML)(NNs)_2}]^-$, as revealed by negative-mode electrospray ionization high-resolution mass spectrometry (ESI-HRMS$^-$) analysis. Upon addition of 10 equiv of PhINNs to $\mathbf{PPh_4[Co^{III}(TAML^{red})]}$ in CH_2Cl_2 or toluene at r.t., quantitative formation on bis-nitrene species $[\mathbf{Co(TAML)(NNs)_2}]^-$ was achieved on the basis of ESI-HRMS$^-$ and UV−vis analysis (Scheme 4 and Figure 6A,B).[41] Although bis-nitrene formation was readily achieved for the anionic complex upon addition of excess PhINNs, the addition of 10 equiv of PhINNs to neutral complex $[\mathbf{Co^{III}(TAML^{sq})}]$ in CH_2Cl_2 or toluene at r.t. led to the quantitative formation of only mononitrene species $[\mathbf{Co(TAML)(NNs)}]$, as shown by ESI-HRMS$^-$ and UV−vis analysis (Scheme 4 and Figure 6C,D). Also, the addition of alternative nitrene source PhINTs (10 equiv) to $[\mathbf{Co^{III}(TAML^{sq})}]$ in CH_2Cl_2 or toluene at room temperature led to the formation of mononitrene complex $[\mathbf{Co(TAML)(NTs)}]$, according to ESI-HRMS$^-$ data. The effective magnetic moments of $[\mathbf{Co(TAML)(NNs)_2}]^-$ ($2.75\mu_B$) and $[\mathbf{Co(TAML)(NNs)}]$ ($1.53\mu_B$) are consistent

Scheme 4. Synthesis of Bis-nitrene (Radical) Complex $\mathbf{PPh_4[Co^{III}(TAML^{q})(NNs)_2]}$ and Mono-nitrene (Radical) Complex $[\mathbf{Co^{III}(TAML^{q})(NR)}]$ (R = Ns, Ts) from $\mathbf{PPh_4[Co^{III}(TAML^{red})]}$ and $[\mathbf{Co^{III}(TAML^{sq})}]$, Respectively

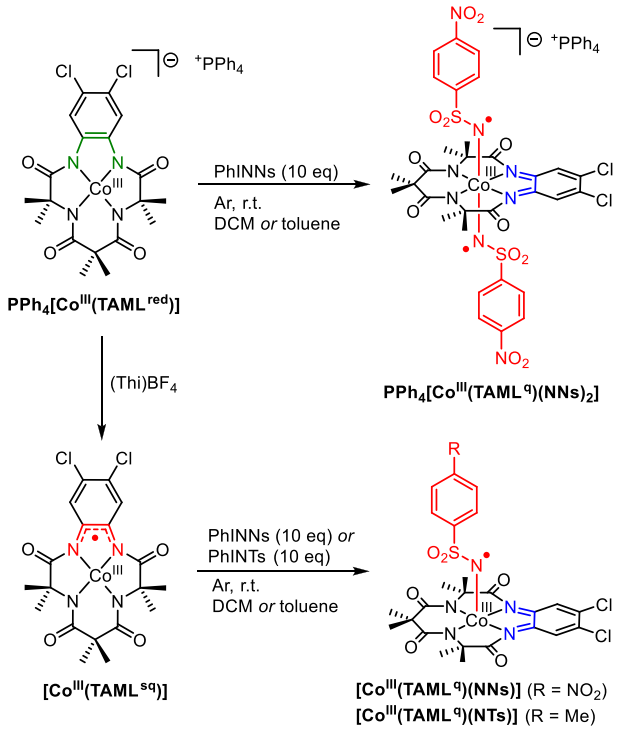

with the formation of (net) triplet ($S = 1$) and doublet ($S = {}^1/_2$) systems, respectively. For clarity, we already included the assigned oxidation states of the ligand and cobalt for anionic bis-nitrene ($[\mathbf{Co^{III}(TAML^{q})(NNs)_2}]^-$) and neutral mononitrene ($[\mathbf{Co^{III}(TAML^{q})(NNs)}]$) in Scheme 4 and Figure 6 and the following text. In the next sections, we will further elaborate on the measurements and calculations leading to these assignments.

As can be expected for an integer spin system, anionic bis-nitrene complex $[\mathbf{Co^{III}(TAML^{q})(NNs)_2}]^-$ is X-band EPR silent at both r.t. and at 10 K. Neutral mononitrene complex $[\mathbf{Co^{III}(TAML^{q})(NNs)}]$ displays an isotropic EPR signal (Figure 7A) at g_{iso} = 2.091 at r.t., showing well-resolved ^{59}Co (A^{Co}_{iso} = 89.5 MHz) and poorly resolved (but necessary for accurate simulation) ^{14}N (A^{N}_{iso} = 18.9 MHz) HFIs. The anisotropic low-temperature (20 K) EPR spectrum of $[\mathbf{Co^{III}(TAML^{q})(NNs)}]$ recorded in toluene glass displays a slightly rhombic signal with small g anisotropy and multiple hyperfine coupling interactions, consistent with a net-doublet ground state (Figure 7B).[42] The r.t. EPR spectrum of $[\mathbf{Co^{III}(TAML^{q})(NTs)}]$ proved to be similar to that of $[\mathbf{Co^{III}(TAML^{q})(NNs)}]$ (SI).

The Co K-edge XANES spectra for $\mathbf{PPh_4[Co^{III}(TAML^{q})(NNs)_2]}$ and $[\mathbf{Co^{III}(TAML^{q})(NNs)}]$ are shown in Figure 8. As was observed for the parent complexes $\mathbf{PPh_4[Co^{III}(TAML^{red})]}$ and $[\mathbf{Co^{III}(TAML^{sq})}]$, the edge position for both cobalt-nitrene complexes is detected at 7721 eV, suggesting that the cobalt centers in all four complexes have the same overall +III oxidation state. Interestingly, the intense shoulder absorption at 7715 eV observed in the spectra of $\mathbf{PPh_4[Co^{III}(TAML^{q})(NNs)_2]}$ and $[\mathbf{Co^{III}(TAML^{q})(NNs)}]$ (corresponding to $1s \rightarrow 4p_z$ + LMCT shakedown transitions characteristic of square planar cobalt complexes) is no longer visible in the nitrene adducts, thus

DOI: 10.1021/jacs.9b11715
J. Am. Chem. Soc. 2020, 142, 552−563

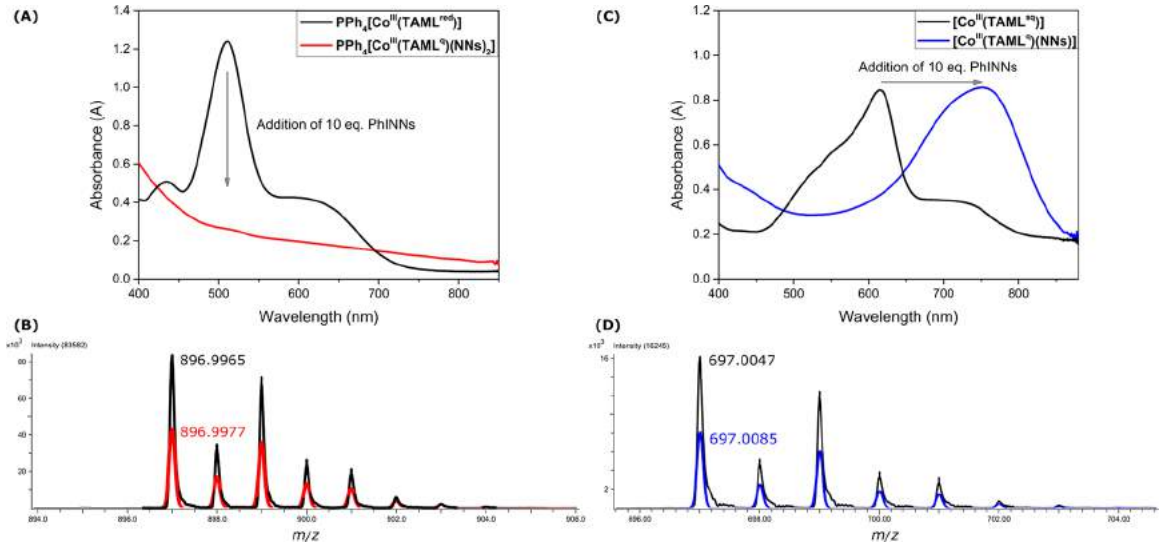

Figure 6. (A) UV−vis spectrum of $\mathbf{PPh_4[Co^{III}(TAML^q)(NNs)_2]}$ (red) upon reaction of $\mathbf{PPh_4[Co^{III}(TAML^{red})]}$ (150 μM in CH_2Cl_2, black) with 10 equiv of PhINNs. (B) ESI-HRMS$^-$ spectrum (black) and simulated spectrum (red) for $\mathbf{[Co^{III}(TAML^q)(NNs)_2]^-}$. (C) UV−vis spectrum of $\mathbf{[Co^{III}(TAML^q)(NNs)]}$ (blue), formed by the addition of 10 equiv of PhINNs to $\mathbf{[Co^{III}(TAML^{sq})]}$ (78 μM in CH_2Cl_2, black). (D) ESI-HRMS$^-$ spectrum (black) and simulated spectrum (blue) for $\mathbf{[Co^{III}(TAML^q)(NNs)]}$.

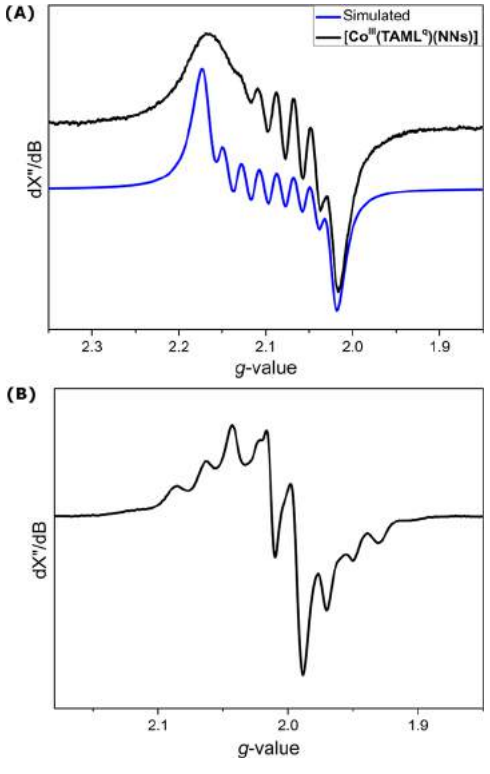

Figure 7. (A) Experimental (black) and simulated (blue) X-band EPR spectra of $\mathbf{[Co^{III}(TAML^q)(NNs)]}$ at r.t. in toluene. Microwave freq. 9.3716 GHz, mod. amp. 2.000 G, and power 6.325 mW. Simulated parameters: g_{iso} = 2.091, $A^{Co}{}_{iso}$ = 89.5 (34.2) MHz, and $A^{N}{}_{iso}$ = 18.9 MHz. (B) X-band EPR spectrum of $\mathbf{[Co^{III}(TAML^q)(NNs)]}$ in toluene glass at 20 K. Microwave freq. 9.376 GHz, mod. amp. 2.000 G, and power 6.325 mW.

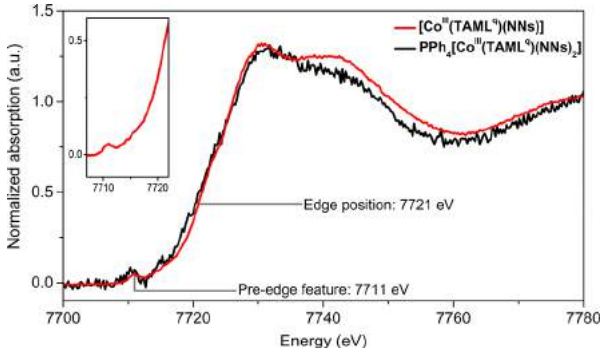

Figure 8. Co K-edge XANES analysis of $\mathbf{PPh_4[Co^{III}(TAML^q)(NNs)_2]}$ (black) and $\mathbf{[Co^{III}(TAML^q)(NNs)]}$ (red) in toluene. (Inset) Close-up of the pre-edge feature for $\mathbf{[Co^{III}(TAML^{sq})(NNs)]}$.

suggesting that both complexes undergo changes in coordination number and/or geometry. This was also observed in related Co^{III}(porphyrin)-mono- and bis-nitrene complexes that displayed an octahedral coordination environment, with an axial coligand ($NsNH_2$, $NsNH^-$, H_2O, or solvent) present in case of the mononitrene species.[14b] Moreover, an additional low-intensity pre-edge feature at 7711 eV is observed clearly for $\mathbf{[Co^{III}(TAML^q)(NNs)]}$ (inset in Figure 8). The pre-edge feature in the XANES spectrum of $\mathbf{PPh_4[Co^{III}(TAML^q)(NNs)_2]}$ is not well-resolved because of moderate data quality caused by low solubility of the complex. These pre-edge features arise from 1s → 3d transitions, and in centrosymmetric (i.e., square planar and octahedral) complexes, these transitions are weak because of quadrupole transitions.[14b] However, symmetry breaking enables 3d−4p hybridization of metal atomic orbitals, causing the pre-edge to gain intensity as a result of dipole-allowed transitions. It thus seems that $\mathbf{[Co^{III}(TAML^q)(NNs)]}$ bears an unidentified sixth coordinating coligand (octahedral coordination geometry) but is not fully centrosymmetric. However, similar low-intensity pre-edge features have been observed in a five-coordinate cobalt-TAML complex;[27] therefore, square pyramidal coordination around cobalt cannot be fully excluded for $\mathbf{[Co^{III}(TAML^q)(NNs)]}$.

Consistent with the above-mentioned experimental results, DFT calculations (BP86, def2-TZVP, disp3, and m4 grid) indicate that the formation of neutral mononitrene complex $\mathbf{[Co^{III}(TAML^q)(NNs)]}$ ($S = {}^1/_2$; $\Delta G^{o}{}_{298\ K} = -20.3$ kcal mol^{-1}) from $\mathbf{[Co^{III}(TAML^{sq})]}$ ($S = {}^1/_2$; reference point) is energetically

DOI: 10.1021/jacs.9b11715
J. Am. Chem. Soc. 2020, 142, 552−563

more favorable than the formation of the neutral bis-nitrene adduct $[\mathbf{Co(TAML)(NNs)_2}]$ ($S = {}^1/_2$; $\Delta G^\circ_{298\ K} = -14.5$ kcal mol^{-1}). However, the corresponding formation energies of the anionic mono- and bis-nitrene complexes $[\mathbf{Co^{III}(TAML^{sq})(NNs)}]^-$ ($S = 1$; $\Delta G^\circ_{298\ K} = -27.9$ kcal mol^{-1}) and $[\mathbf{Co^{III}(TAML^{q})(NNs)_2}]^-$ ($S = 1$; $\Delta G^\circ_{298\ K} = -29.9$ kcal mol^{-1}) from $[\mathbf{Co^{III}(TAML^{red})}]^-$ ($S = 1$; reference point) are nearly equal (SI).

NEVPT2-corrected CASSCF calculations were performed to accurately describe the electronic structure of the nitrene species. All cobalt d orbitals, ligands L_π, and nitrene-localized p orbitals were included in the active spaces. CASSCF(14,13) calculations on $[\mathbf{Co^{III}(TAML^{q})(NNs)_2}]^-$ showed that the d_{xy} orbital is not preserved in the active space (occupancy 2.00)[40] and that the d_{z^2} orbital forms bonding (nitrene-N^1 and -N^2 localized, occupancy 1.94) and antibonding (mostly d_{z^2} localized, occupancy 0.07) combinations with the nitrene N_{p_z} orbitals. The d_{yz} and d_{xz} orbitals are both filled (occupancies 1.97 and 1.95, respectively), and L_π–d_{xz} (occupancy 0.10) is virtually empty. Given that the L_π orbital was doubly filled in $[\mathbf{Co^{III}(TAML^{red})}]^-$ (vide supra), this implies that the formation of $[\mathbf{Co^{III}(TAML^{q})(NNs)_2}]^-$ from $[\mathbf{Co^{III}(TAML^{red})}]^-$ is associated with the two-electron oxidation of the ligand. Interestingly, both nitrene nitrogen atoms bear a single unpaired electron in their N_{p_y}/N_{p_x} orbitals (both occupancies 1.00). The electronic structure is thus best described as $(d_{xy})^{2.00}(d_{yz})^{1.97}(d_{xz})^{1.95}(N^1_{p_z} + N^2_{p_z} + d_{z^2})^{1.94}(N^2_{p_x})^{1.00}(N^1_{p_y})^{1.00}$, consistent with a Co^{III} center, a fully oxidized TAML backbone ($TAML^q$), and two one-electron-reduced Fischer-type nitrene radical substrates ($N^\bullet Ns^-$).[43] Moreover, the cobalt(III) center has undergone a spin transition from intermediate spin in $[\mathbf{Co^{III}(TAML^{red})}]^-$ to low spin in $[\mathbf{Co^{III}(TAML^{q})(N^\bullet Ns^-)_2}]^-$ upon formation of the bis-nitrene radical species. As a result, the net total spin state does not change in the process and remains a triplet spin state ($S = 1$). The most relevant active orbitals and their occupation numbers are shown in Figure 9A. In addition, excitation energies derived from the CASSCF(14,13) calculation revealed that no intense absorption bands are expected in the 400–850 nm region (SI), consistent with the experimental spectrum depicted in Figure 6A.

The complex bears some resemblance to the previously reported cobalt-porphyrin bis-nitrene ($[Co^{III}(TPP^{\bullet-})(N^\bullet Ns^-)_2]$)[14] and ruthenium-porphyrin bis-imido ($[Ru^{VI}(TPP)(NTs)_2]$)[44] complexes (TPP = tetraphenylporphyrin). The ruthenium bis-imido complex is formed exclusively via metal-centered oxidation processes. However, whereas in the cobalt-porphyrin complex double nitrene-radical formation is the result of combined metal-to-substrate and (porphyrin) ligand-to-substrate SET processes, the formation of $[\mathbf{Co^{III}(TAML^{q})(N^\bullet Ns^-)_2}]^-$ is an entirely (double) ligand-to-substrate single-electron-transfer process.

In a very similar fashion, CASSCF(13,12) calculations on $[\mathbf{Co^{III}(TAML^{q})(NNs)}]$ reveal π (d_{yz}+ N_{p_y}) and σ (d_{z^2}+ N_{p_z}) bonding interactions between cobalt and the nitrene, with occupations of 1.93 and 1.86 electrons, respectively.[45] The d_{xz} orbital is filled (occupancy 1.91), and the formerly half-filled L_π–d_{xz} orbital is now unoccupied (occupancy 0.12), indicating single-electron oxidation of the ligand (i.e., from $\mathbf{TAML^{sq}}$ to $\mathbf{TAML^{q}}$). The single unpaired electron of the complex is mainly localized on the nitrene moiety (N_{p_y}–d_{yz}, occupancy 1.06), again consistent with $[\mathbf{Co^{III}(TAML^{q})(N^\bullet Ns^-)}]$ being a Fischer-type nitrene radical complex with net π-bond order between cobalt and the nitrene of ~0.5.[43] As for the anionic bis-nitrene complex, the neutral mononitrene complex is generated via ligand-to-substrate SET. Once again, the cobalt(III) ion does not change its oxidation state in the process, but it does undergo a spin flip from intermediate spin in $[\mathbf{Co^{III}(TAML^{sq})}]$ to low spin in $[\mathbf{Co^{III}(TAML^{q})(N^\bullet Ns^-)}]$. The most relevant active orbitals and their occupations are shown in Figure 9B. Notably, neither $[\mathbf{Co^{III}(TAML^{q})(N^\bullet Ns^-)_2}]^-$ nor $[\mathbf{Co^{III}(TAML^{q})(N^\bullet Ns^-)}]$ has significant multireference character.

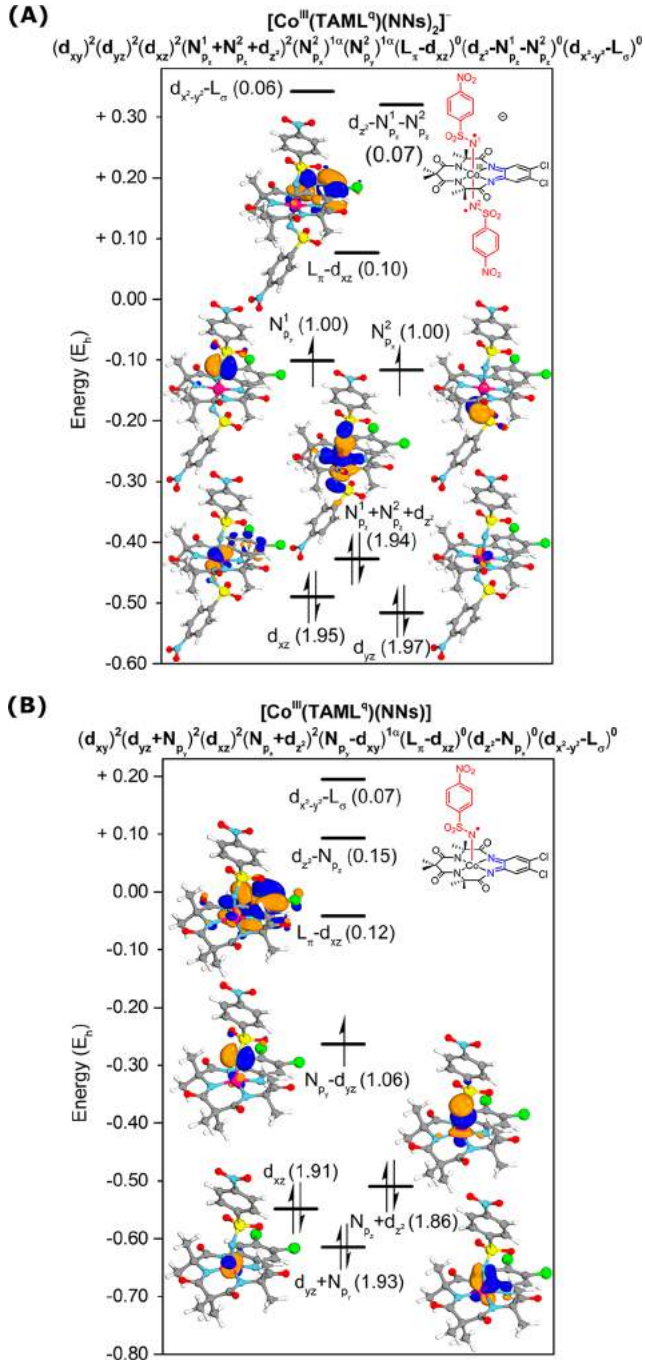

Figure 9. Most relevant active orbitals and occupancies (in parentheses) of NEVPT2-corrected CASSCF(14,13) ($[\mathbf{Co^{III}(TAML^{q})(NNs)_2}]^-$) (A) and CASSCF(13,12) ($[\mathbf{Co^{III}(TAML^{q})(NNs)}]$) (B) calculations.

DOI: 10.1021/jacs.9b11715
J. Am. Chem. Soc. 2020, 142, 552–563

Interestingly, ligand-to-substrate SET combined with a metal-based spin flip effectively leads to a shift in the spin density from the metal to the nitrene nitrogen(s) in both the neutral mononitrene and the anionic bis-nitrene complexes, without the oxidation of cobalt and without changing the net total spin state of the complex. The redox events clearly occur on the TAML backbone (electron donor) and the nitrene (electron acceptor), wherein the former undergoes one-electron or two-electron oxidation to accommodate one or two nitrene radicals on the Co^{III} center.

Intrigued by the influence of the ligand oxidation state on the structure of the nitrene species, the mono- and bis-nitrene species were probed for catalytic nitrene transfer reactivity in the benchmark aziridination of styrene (Scheme 5).[1a,3] A remarkable difference in the yield of aziridine product **1** was observed when using $\mathbf{PPh_4[Co^{III}(TAML^{red})]}$ (64%) or $\mathbf{[Co^{III}(TAML^{sq})]}$ (35%) as the catalyst in nitrene transfer reactions from PhINNs to styrene, suggesting that the anionic bis-nitrene and neutral mononitrene exhibit markedly different activity and/or stability properties. A thorough investigation of the applicability and mechanisms of $\mathbf{PPh_4[Co^{III}(TAML^{red})]}$ and $\mathbf{[Co^{III}(TAML^{sq})]}$ as aziridination catalysts is the subject of current investigations, which will be reported in due time. At this point it is worth mentioning that for cobalt-TAML complexes the reduced (anionic) $\mathbf{[Co^{III}(TAML^{red})]^-}$ species are apparently more effective nitrene-transfer catalysts than the corresponding oxidized (neutral) $\mathbf{[Co^{III}(TAML^{sq})]}$ species, while for iron- and manganese-TAML complexes the reverse was observed.[19,20]

Scheme 5. Catalytic Aziridination of Styrene to Afford 1 Using $\mathbf{PPh_4[Co^{III}(TAML^{red})]}$ and $\mathbf{[Co^{III}(TAML^{sq})]}$

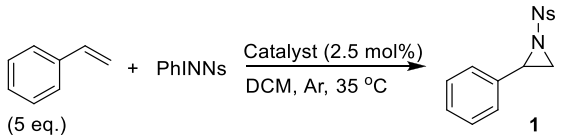

$\mathbf{PPh_4[Co^{III}(TAML^{red})]}$	64%
$\mathbf{[Co^{III}(TAML^{sq})]}$	35%

CONCLUSIONS

In this work we have conclusively shown that the ligand in Co(TAML) complexes is redox-active. The oxidation of $\mathbf{[Co^{III}(TAML^{red})]^-}$ using (Thi)BF_4 cleanly affords $\mathbf{[Co^{III}(TAML^{sq})]}$ via ligand-centered oxidation, with the electronic structure being best described as an intermediate spin ($S = 1$) cobalt(III) center that is antiferromagnetically coupled to a ligand-centered radical ($S = {}^1/_2$).

Interestingly, cobalt-nitrene adducts of $\mathbf{PPh_4[Co^{III}(TAML^{red})]}$ and $\mathbf{Co^{III}(TAML^{sq})}$ can be cleanly generated from PhINNs via ligand-to-substrate single-electron transfer to afford $\mathbf{PPh_4[Co^{III}(TAML^{q})(NNs)_2]^-}$ and $\mathbf{[Co^{III}(TAML^{q})(NNs)]}$, respectively. CASSCF calculations revealed that both nitrene complexes are best described as one-electron-reduced Fischer-type nitrene radicals. The formation of a bis-nitrene adduct of $\mathbf{PPh_4[Co^{III}(TAML^{red})]}$ is attributed to the availability of two electrons within the reduced TAML framework for double ligand-to-substrate SET, whereas only one electron can be used for ligand-to-substrate SET on $\mathbf{[Co^{III}(TAML^{sq})]}$, which therefore affords the mononitrene adduct. Intriguingly, in both cases the combination of ligand-to-substrate SET and a spin flip from intermediate spin ($S = 1$) to low spin ($S = 0$) at the cobalt(III) center effectively results in a shift of the spin density from the metal to the nitrene moieties, without the oxidation of cobalt and without changing the net total spin state of the complex.

Preliminary catalytic styrene aziridination reactions using $\mathbf{PPh_4[Co^{III}(TAML^{red})]}$ or $\mathbf{[Co^{III}(TAML^{sq})]}$ as the catalyst reveal remarkable differences in activity/stability between the two systems. More elaborate studies on the underlying mechanisms, synthesis applicability, and differences between the two complexes in nitrene transfer catalysis will be reported in the near future.

ASSOCIATED CONTENT

Supporting Information

The Supporting Information is available free of charge at https://pubs.acs.org/doi/10.1021/jacs.9b11715.

X-ray structure of $TAMLH_4$ (CIF)

X-ray structure of $PPh_4[Co_{III}(TAML_{red})]$ (CIF)

Experimental details; synthesis procedures; relevant NMR, EPR, HRMS, XRD, UV−vis, electrochemical, and XANES data; geometries (*xyz* coordinates) of stationary points (DFT); and a description of the CASSCF calculations (PDF)

AUTHOR INFORMATION

Corresponding Authors

*j.i.vandervlugt@uva.nl

*b.debruin@uva.nl

ORCID

Maxime A. Siegler: 0000-0003-4165-7810

Moniek Tromp: 0000-0002-7653-1639

Jarl Ivar van der Vlugt: 0000-0003-0665-9239

Bas de Bruin: 0000-0002-3482-7669

Notes

The authors declare no competing financial interest.

ACKNOWLEDGMENTS

Financial support from The Netherlands Organization for Scientific Research (NWO TOP-Grant 716.015.001 to B.d.B. and NWO VIDI grant 723.014.010 to M.T.) is gratefully acknowledged. We thank Ed Zuidinga for HRMS measurements and Lars Grooten for preliminary UV−vis studies. The authors thank the staff of beamline B18, Diamond Light Source (proposal number SP22432) in Didcot, U.K. for support and access to their facilities.

REFERENCES

(1) (a) van Leest, N. P.; Epping, P. F. J.; van Vliet, K. M.; Lankelma, M.; van den Heuvel, E. J.; Heijtbrink, N.; Broersen, R.; de Bruin, B. Single-Electron Elementary Steps in Homogeneous Organometallic Catalysis. *Advances in Organometallic Chemistry*; Elsevier: London, 2018; Vol. *70*, pp 71−180. (b) Broere, D. L. J.; Plessius, R.; van der Vlugt, J. I. New avenues for ligand-mediated processes - expanding metal reactivity by the use of redox-active catechol, *o*-aminophenol and *o*-phenylenediamine ligands. *Chem. Soc. Rev.* **2015**, *44*, 6886−6915. (c) Chirila, A.; Das, B. G.; Kuijpers, P. F.; Sinha, V.; de Bruin, B. Application of Stimuli-Responsive and "Non-Innocent" Ligands in Base Metal Catalysis. In *Non-Noble Metal Catalysis Molecular Approaches and Reactions*; Wiley-VCH Verlag GmbH & Co. KGaA: Weinheim, Germany, 2018; pp 1−31. (d) Lu, H.; Zhang, X. P. Catalytic C-H functionalization by metalloporphyrins: recent developments and future directions. *Chem. Soc. Rev.* **2011**, *40*, 1899−1909. (e) Lyaskov-

DOI: 10.1021/jacs.9b11715
J. Am. Chem. Soc. 2020, 142, 552−563

skyy, V.; de Bruin, B. Redox Non-innocent Ligands − Versatile New Tools to Control Catalytic Reactions. *ACS Catal.* **2012**, *2*, 270−279.
(2) Hili, R.; Yudin, A. K. Making carbon-nitrogen bonds in biological and chemical synthesis. *Nat. Chem. Biol.* **2006**, *2*, 284−287.
(3) (a) Kuijpers, P. F.; van der Vlugt, J. I.; Schneider, S.; de Bruin, B. Nitrene Radical Intermediates in Catalytic Synthesis. *Chem. - Eur. J.* **2017**, *23*, 13819−13829. (b) Park, Y.; Kim, Y.; Chang, S. Transition Metal-Catalyzed C−H Amination: Scope, Mechanism, and Applications. *Chem. Rev.* **2017**, *117*, 9247−9301. (c) Shin, K.; Kim, H.; Chang, S. Transition-Metal-Catalyzed C−N Bond Forming Reactions Using Organic Azides as the Nitrogen Source: A Journey for the Mild and Versatile C−H Amination. *Acc. Chem. Res.* **2015**, *48*, 1040−1052.
(4) (a) Intrieri, D.; Carminati, D. M.; Gallo, E. Recent advances in C−H bond aminations catalyzed by ruthenium porphyrin complexes. *J. Porphyrins Phthalocyanines* **2016**, *20*, 190−203. (b) Zardi, P.; Caselli, A.; Macchi, P.; Ferretti, F.; Gallo, E. Synthesis of Biologically Relevant Compounds by Ruthenium Porphyrin Catalyzed Amination of Benzylic C−H Bonds. *Organometallics* **2014**, *33*, 2210−2218. (c) Fantauzzi, S.; Gallo, E.; Caselli, A.; Ragaini, F.; Casati, N.; Macchi, P.; Cenini, S. The key intermediate in the amination of saturated C−H bonds: synthesis, X-ray characterization and catalytic activity of $Ru(TPP)(NAr)_2$ (Ar = $3,5\text{-}(CF_3)_2C_6H_3$). *Chem. Commun.* **2009**, 3952−3954.
(5) (a) Guthikonda, K.; When, P. M.; Caliando, B. J.; Du Bois, J. Rh-catalyzed alkene oxidation: a highly efficient and selective process for preparing N-alkoxysulfonyl aziridines. *Tetrahedron* **2006**, *62*, 11331−11342. (b) Liang, C.; Robert-Peillard, F.; Fruit, C.; Müller, P.; Dodd, R. H.; Dauban, P. Efficient Diastereoselective Intermolecular Rhodium-Catalyzed C-H Amination. *Angew. Chem., Int. Ed.* **2006**, *45*, 4641−4644. (c) Espino, C. G.; When, P. M.; Chow, J.; Du Bois, J. Synthesis of 1,3-Difunctionalized Amine Derivatives through Selective C−H Bond Oxidation. *J. Am. Chem. Soc.* **2001**, *123*, 6935−6936. (d) Roizen, J. L.; Zalatan, D. N.; De Bois, J. Selective Intermolecular Amination of C-H Bonds at Tertiary Carbon Centers. *Angew. Chem., Int. Ed.* **2013**, *52*, 11343−11346.
(6) (a) Broere, D. L. J.; de Bruin, B.; Reek, J. N. H.; Lutz, M.; Dechert, S.; van der Vlugt, J. I. Intramolecular Redox-Active Ligand-to-Substrate Single-Electron Transfer: Radical Reactivity with a Palladium(II) Complex. *J. Am. Chem. Soc.* **2014**, *136*, 11574−11577. (b) Broere, D. L. J.; van Leest, N. P.; de Bruin, B.; Siegler, M. A.; van der Vlugt, J. I. Reversible Redox Chemistry and Catalytic C(sp^3)−H Amination Reactivity of a Paramagnetic Pd Complex Bearing a Redox-Active *o*-Aminophenol-Derived NNO Pincer Ligand. *Inorg. Chem.* **2016**, *55*, 8603−8611. (c) Okamoto, K.; Oda, T.; Kohigashi, S.; Ohe, K. Palladium-Catalyzed Decarboxylative Intramolecular Aziridination from 4*H*-Isoxazol-5-ones Leading to 1-Azabicyclo[3.1.0]hex-2-enes. *Angew. Chem., Int. Ed.* **2011**, *50*, 11470−11473.
(7) (a) Llaveria, J.; Beltrán, Á.; Díaz-Requejo, M. M.; Matheu, M. I.; Castillón, S.; Pérez, P. J. Efficient Silver-Catalyzed Regio- and Stereospecific Aziridination of Dienes. *Angew. Chem., Int. Ed.* **2010**, *49*, 7092−7095. (b) Rigoli, J. W.; Weatherly, C. D.; Alderson, J. M.; Vo, B. T.; Schomaker, J. M. Tunable, Chemoselective Amination via Silver Catalysis. *J. Am. Chem. Soc.* **2013**, *135*, 17238−17241. (c) Dolan, N. S.; Scamp, R. J.; Yang, T.; Berry, J. F.; Schomaker, J. M. Catalyst-Controlled and Tunable, Chemoselective Silver-Catalyzed Intermolecular Nitrene Transfer: Experimental and Computational Studies. *J. Am. Chem. Soc.* **2016**, *138*, 14658−14667. (d) Cui, Y.; He, C. Efficient Aziridination of Olefins Catalyzed by a Unique Disilver(I) Compound. *J. Am. Chem. Soc.* **2003**, *125*, 16202−16203.
(8) Li, Z.; Ding, X.; He, C. Nitrene Transfer Reactions Catalyzed by Gold Complexes. *J. Org. Chem.* **2006**, *71*, 5876−5880.
(9) (a) Minakata, S.; Ando, T.; Nishimura, M.; Ryu, I.; Komatsu, M. Novel Asymmetric and Stereospecific Aziridination of Alkenes with a Chiral Nitridomanganese Complex. *Angew. Chem., Int. Ed.* **1998**, *37*, 3392−3394. (b) Nishikori, H.; Katsuki, T. Catalytic and highly enantioselective aziridination of styrene derivatives. *Tetrahedron Lett.* **1996**, *37*, 9245−9248. (c) Yang, J.; Weinberg, R.; Breslow, R. The hydroxylation and amidation of equilenin acetate catalyzed by chloro[5,10,15,20-tetrakis(pentafluorophenyl)porphyrinato]-manganese(III). *Chem. Commun.* **2000**, 531−532.
(10) (a) Bagh, B.; Broere, D. L. J.; Sinha, V.; Kuijpers, P. F.; van Leest, N. P.; de Bruin, B.; Demeshko, S.; Siegler, M. A.; van der Vlugt, J. I. Catalytic Synthesis of N-Heterocycles via Direct C(sp^3)−H Amination Using an Air-Stable Iron(III) Species with a Redox-Active Ligand. *J. Am. Chem. Soc.* **2017**, *139*, 5117−5124. (b) Avenier, F.; Latour, J.-M. Catalytic aziridination of olefins and amidation of thioanisole by a non-heme iron complex. *Chem. Commun.* **2004**, 1544−1545. (c) Fingerhut, A.; Serdyuk, O. V.; Tsogoeva, S. B. Non-heme iron catalysts for epoxidation and aziridination reactions of challenging terminal alkenes: towards sustainability. *Green Chem.* **2015**, *17*, 2042−2058. (d) Correa, A.; Mancheño, O. G.; Bolm, C. Iron-catalysed carbon−heteroatom and heteroatom−heteroatom bond forming processes. *Chem. Soc. Rev.* **2008**, *37*, 1108−1117. (e) Hennessy, E. T.; Betley, T. A. Complex N-Heterocycle Synthesis via Iron-Catalyzed, Direct C-H Bond Amination. *Science* **2013**, *340*, 591−595. (f) Iovan, D. A.; Betley, T. A. Characterization of Iron-Imido Species Relevant for N-Group Transfer Chemistry. *J. Am. Chem. Soc.* **2016**, *138*, 1983−1993. (g) Patra, R.; Coin, G.; Castro, L.; Dubourdeaux, P.; Clémancey, M.; Pécaut, J.; Lebrun, C.; Maldivi, L. J.-M. Rational design of Fe catalysts for olefin aziridination through DFT-based mechanistic analysis. *Catal. Sci. Technol.* **2017**, *7*, 4388−4400. (h) Klotz, K. L.; Slominksi, L. M.; Hull, A. V.; Gottsacker, V. M.; Mas-Ballesté, R.; Que, L., Jr.; Halfen, J. A. Non-heme iron(II) complexes are efficient olefin aziridination catalysts. *Chem. Commun.* **2007**, 2063−2065. (i) Klotz, K. L.; Slominski, L. M.; Riemer, M. E.; Phillips, J. A.; Halfen, J. A. Mechanism of the Iron-Mediated Alkene Aziridination Reaction: Experimental and Computational Investigations. *Inorg. Chem.* **2009**, *48*, 801−803. (j) Chandrachud, P. P.; Bass, H. M.; Jenkins, D. M. Synthesis of Fully Aliphatic Aziridines with a Macrocyclic Tetracarbene Iron Catalyst. *Organometallics* **2016**, *35*, 1652−1657. (k) Nakanishi, M.; Salit, A.-F.; Bolm, C. Iron-Catalyzed Aziridination Reactions. *Adv. Synth. Catal.* **2008**, *350*, 1835−1840.
(11) (a) Kuijpers, P. F.; Tiekink, M. J.; Breukelaar, W. B.; Broere, D. L. J.; van Leest, N. P.; van der Vlugt, J. I.; Reek, J. N. H.; de Bruin, B. Cobalt-Porphyrin-Catalysed Intramolecular Ring-Closing C−H Amination of Aliphatic Azides: A Nitrene-Radical Approach to Saturated Heterocycles. *Chem. - Eur. J.* **2017**, *23*, 7945−7952. (b) Goswami, M.; Geuijen, P.; Reek, J. N. H.; de Bruin, B. Application of [Co(Corrole)]-Complexes in Ring-Closing C-H Amination of Aliphatic Azides via Nitrene Radical Intermediates. *Eur. J. Inorg. Chem.* **2018**, *2018*, 617−626. (c) Baek, Y.; Betley, T. A. Catalytic C−H Amination Mediated by Dipyrrin Cobalt Imidos. *J. Am. Chem. Soc.* **2019**, *141*, 7797−7806. (d) Jin, L.-M.; Lu, H.; Cui, Y.; Lizardi, C. L.; Arzua, T. N.; Wojtas, L.; Cui, X.; Zhang, X. P. Selective radical amination of aldehydic C(sp2)−H bonds with fluoroaryl azides via Co(II)-based metalloradical catalysis: synthesis of N-fluoroaryl amides from aldehydes under neutral and nonoxidative conditions. *Chem. Sci.* **2014**, *5*, 2422−2427. (e) Lu, H.; Jiang, H.; Wojtas, L.; Zhang, X. P. *Angew. Chem., Int. Ed.* **2010**, *49*, 10192−10196. (f) Ruppel, J. V.; Kamble, R. M.; Zhang, X. P. Selective Intramolecular C-H Amination through the Metalloradical Activation of Azides: Synthesis of 1,3-Diamines under Neutral and Nonoxidative Conditions. *Org. Lett.* **2007**, *9*, 4889−4892. (g) Jin, L.-M.; Xu, X.; Lu, H.; Cui, X.; Wojtas, L.; Zhang, X. P. Effective Synthesis of Chiral *N*-Fluoroaryl Aziridines through Enantioselective Aziridination of Alkenes with Fluoroaryl Azides. *Angew. Chem., Int. Ed.* **2013**, *52*, 5309−5313. (h) Gao, G.-Y.; Jones, J. E.; Vyas, R.; Harden, J. D.; Zhang, X. P. *J.* Cobalt-Catalyzed Aziridination with Diphenylphosphoryl Azide (DPPA): Direct Synthesis of *N*-Phosphorus-Substituted Aziridines from Alkenes. *J. Org. Chem.* **2006**, *71*, 6655−6658. (i) Subbarayan, V.; Ruppel, J. V.; Zhu, S.; Perman, J. A.; Zhang, X. P. Highly asymmetric cobalt-catalyzed aziridination of alkenes with trichloroethoxysulfonyl azide ($TcesN_3$). *Chem. Commun.* **2009**, 4266−4268. (j) Gao, G.-Y.; Harden, J. D.; Zhang, X. P. Cobalt-Catalyzed Efficient Aziridination of Alkenes. *Org. Lett.* **2005**, *7*, 3191−3193. (k) Caselli, A.; Gallo, E.; Fantauzzi, S.; Morlacchi, S.; Ragaini, F.; Cenini, S. Allylic Amination and Aziridination of Olefins by Aryl Azides Catalyzed by Co^{II}(tpp): A Synthetic and Mechanistic Study. *Eur. J. Inorg. Chem.* **2008**, *2008*, 3009−3019.

DOI: 10.1021/jacs.9b11715
J. Am. Chem. Soc. 2020, 142, 552−563

(12) (a) Wiese, S.; Aguila, M. J. B.; Kogut, E.; Warren, T. H. β-Diketiminato Nickel Imides in Catalytic Nitrene Transfer to Isocyanides. *Organometallics* **2013**, *32*, 2300−2308. (b) Iluc, V. M.; Miller, A. J. M.; Anderson, J. S.; Monreal, M. J.; Mehn, M. P.; Hillhouse, G. L. Synthesis and Characterization of Three-Coordinate Ni(III)-Imide Complexes. *J. Am. Chem. Soc.* **2011**, *133*, 13055−13063. (c) Kogut, E.; Wiencko, H. L.; Zhang, L.; Cordeau, D. E.; Warren, T. H. A Terminal Ni(III)−Imide with Diverse Reactivity Pathways. *J. Am. Chem. Soc.* **2005**, *127*, 11248−11249.

(13) (a) van Vliet, K. M.; Polak, L. H.; Sieglet, M. A.; van der Vlugt, J. I.; Fonseca Guerra, C.; de Bruin, B. Efficient Copper-Catalyzed Multicomponent Synthesis of N-Acyl Amidines via Acyl Nitrenes. *J. Am. Chem. Soc.* **2019**, *141*, 15240−15249. (b) Carsch, K. M.; DiMucci, I. M.; Iovan, D. A.; Li, A.; Zheng, S.-L.; Titus, C. J.; Lee, S. J.; Irwin, K. V.; Nordlund, D.; Lancaster, K. M.; Betley, T. A. Synthesis of a copper-supported triplet nitrene complex pertinent to copper-catalyzed amination. *Science* **2019**, *365*, 1138−1143. (c) Evans, D. A.; Faul, M. M.; Bilodeau, M. T.; Anderson, B. A.; Barnes, D. M. Bis(oxazoline)-copper complexes as chiral catalysts for the enantioselective aziridination of olefins. *J. Am. Chem. Soc.* **1993**, *115*, 5328−5329. (d) Li, Z.; Quan, R. W.; Jacobsen, E. N. Mechanism of the (Diimine)copper-Catalyzed Asymmetric Aziridination of Alkenes. Nitrene Transfer via Ligand-Accelerated Catalysis. *J. Am. Chem. Soc.* **1995**, *117*, 5889−5890. (e) Gephart, R. T.; III; Warren, T. H. Copper-Catalyzed sp3 C−H Amination. *Organometallics* **2012**, *31*, 7728−7752. (f) Lebel, H.; Parmentier, M. Copper-catalyzed enantioselective aziridination of styrenes. *Pure Appl. Chem.* **2010**, *82*, 1827−1833. (g) Mairena, M. A.; Díaz-Requejo, M. M.; Belderraín, R. R.; Nicasio, M. C.; Trofimenko, S.; Pérez, P. J. Copper-Homoscorpionate Complexes as Very Active Catalysts for the Olefin Aziridination Reaction. *Organometallics* **2004**, *23*, 253−256. (h) Bagchi, V.; Paraskevopoulou, P.; Das, P.; Chi, L.; Wang, Q.; Choudhury, A.; Mathieson, J. S.; Cronin, L.; Pardue, D. B.; Cundari, T. R.; Mitrikas, G.; Sanakis, Y.; Stavropoulos, R. A Versatile Tripodal Cu(I) Reagent for C−N Bond Construction via Nitrene-Transfer Chemistry: Catalytic Perspectives and Mechanistic Insights on C−H Aminations/Amidinations and Olefin Aziridinations. *J. Am. Chem. Soc.* **2014**, *136*, 11362−11381. (i) Ren, Y.; Cheaib, K.; Jacquet, J.; Vezin, H.; Fensterbank, L.; Orio, M.; Blanchard, S.; Desage-El Murr, M. Copper-Catalyzed Aziridination with Redox-Active Ligands: Molecular Spin Catalysis. *Chem. - Eur. J.* **2018**, *24*, 5086−5090.

(14) (a) Lyaskovskyy, V.; Suarez, A. I. O.; Lu, H.; Jiang, H.; Zhang, X. P.; de Bruin, B. Mechanism of Cobalt(II) Porphyrin-Catalyzed C−H Amination with Organic Azides: Radical Nature and H-Atom Abstraction Ability of the Key Cobalt(III)−Nitrene Intermediates. *J. Am. Chem. Soc.* **2011**, *133*, 12264−12273. (b) Goswami, M.; Lyaskobskyy, V.; Domingos, S. R.; Buma, W. J.; Woutersen, S.; Troeppner, O.; Ivanović-Burmazović, I.; Lu, H.; Cui, X.; Zhang, X. P.; Reijerse, E. J.; DeBeer, S.; van Schooneveld, M. M.; Pfaff, F. F.; Ray, K.; de Bruin, B. Characterization of Porphyrin-Co(III)-'Nitrene Radical' Species Relevant in Catalytic Nitrene Transfer Reactions. *J. Am. Chem. Soc.* **2015**, *137*, 5468−5479.

(15) van der Vlugt, J. I. Radical-Type Reactivity and Catalysis by Single-Electron Transfer to or from Redox-Active Ligands. *Chem. - Eur. J.* **2019**, *25*, 2651−2662.

(16) Collins, T. J.; Ryabov, A. D. Targeting of High-Valent Iron-TAML Activators at Hydrocarbons and Beyond. *Chem. Rev.* **2017**, *117*, 9140−9162.

(17) Dutta, S. K.; Beckmann, U.; Bill, E.; Weyhermuller, T.; Wieghardt, K. 1,2-Bis(pyridine-2-carboxamido)benzenate(2−), $(bpb)^{2-}$: A Noninnocent Ligand. Syntheses, Structures, and Mechanisms of Formation of $[(n\text{-}Bu)_4N][Fe^{IV}{}_2(\mu\text{-}N)(bpb)_2(X)_2]$ (X = CN-, N_3-) and the Electronic Structures of $[M^{III}(bpb^{ox1})(CN)_2]$ (M = Co, Fe). *Inorg. Chem.* **2000**, *39*, 3355−3364.

(18) Popescu, D.-L.; Chanda, A.; Stadler, M.; Tiago de Oliveira, F.; Ryabov, A. D.; Münck, E.; Bominaar, E. L.; Collins, T. J. High-valent first-row transition-metal complexes of tetraamido (4N) and diamidodialkoxido or diamidophenolato (2N/2O) ligands: Synthesis, structure, and magnetochemistry. *Coord. Chem. Rev.* **2008**, *252*, 2050−2071.

(19) (a) Hong, S.; Sutherlin, K. D.; Vardhaman, A. K.; Yan, J. J.; Park, S.; Lee, Y.-M.; Jang, S.; Lu, X.; Ohta, T.; Ogura, T.; Solomon, E. I.; Nam, W. A Mononuclear Nonheme Iron(V)-Imido Complex. *J. Am. Chem. Soc.* **2017**, *139*, 8800−8803. (b) Hong, S.; Lu, X.; Lee, Y.-M.; Seo, M. S.; Ohta, T.; Ogura, T.; Clémancey, M.; Maldivi, P.; Latour, J.-M.; Sarangi, R.; Nam, W. Achieving One-Electron Oxidation of a Mononuclear Nonheme Iron(V)-Imido Complex. *J. Am. Chem. Soc.* **2017**, *139*, 14372−14375.

(20) Shi, H.; Xie, J.; Lam, W. W. Y.; Mab, W.-L.; Mak, C.-K.; Yiu, S.-M.; Lee, H. K.; Lau, T.-C. Generation and Reactivity of a One-Electron-Oxidized Manganese(V) Imido Complex with a Tetraamido Macrocyclic Ligand. *Chem. - Eur. J.* **2019**, *25*, 12895−12899.

(21) Collins, T. J.; Powell, R. D.; Slebodnick, C.; Uffelman, E. S. Stable highly oxidizing cobalt complexes of macrocyclic ligands. *J. Am. Chem. Soc.* **1991**, *113*, 8419−8425.

(22) Das, D.; Pattanayak, S.; Singh, K. K.; Garai, B.; Gupta, S. S. Electrocatalytic water oxidation by a molecular cobalt complex through a high valent cobalt oxo intermediate. *Chem. Commun.* **2016**, *52*, 11787−11790.

(23) Du, H.-Y.; Chen, S.-C.; Su, X.-J.; Jiao, L.; Zhang, M.-T. Redox-Active Ligand Assisted Multielectron Catalysis: A Case of Co^{III} Complex as Water Oxidation Catalyst. *J. Am. Chem. Soc.* **2018**, *140*, 1557−1565.

(24) Nasini, U. B.; Gartia, Y.; Ramidi, P.; Kazi, A.; Shaikh, A. U.; Ghosh, A. Oxygen reduction reaction catalyzed by cobalt(III) complexes of macrocyclic ligands supported on multiwalled carbon nanotubes. *Chem. Phys. Lett.* **2013**, *566*, 38−43.

(25) Ghosh, A.; Ramidi, P.; Pulla, S.; Sullivan, S. Z.; Collom, S. L.; Gartia, Y.; Munshi, P.; Biris, A. S.; Noll, B. C.; Berry, B. C. Cycloaddition of CO_2 to Epoxides Using a Highly Active Co(III) Complex of Tetraamidomacrocyclic Ligand. *Catal. Lett.* **2010**, *137*, 1−7.

(26) Parnell, C. M.; Watanabe, F.; Nasini, U. B.; Berry, B. C.; Mitchell, T.; Shaikh, A. U.; Ghosh, A. Electrochemical sensing of hydrogen peroxide using a cobalt(III) complex supported on carbonaceous nanomaterials. *J. Electroanal. Chem.* **2015**, *740*, 37−44.

(27) Hong, S.; Pfaff, F. F.; Kwon, E.; Wang, Y.; Seo, M.-S.; Bill, E.; Ray, K.; Nam, W. Spectroscopic Capture and Reactivity of a Low-Spin Cobalt(IV)-Oxo Complex Stabilized by Binding Redox-Inactive Metal Ions. *Angew. Chem., Int. Ed.* **2014**, *53*, 10403−10407.

(28) Patterson, R. E.; Gordon-Wylie, S. W.; Woomer, C. G.; Norman, R. E.; Weintraub, S. T.; Horwitz, C. P.; Collins, T. J. Electron-Transfer Oxidation by Phase-Separating Reagents. *Inorg. Chem.* **1998**, *37*, 4748−4750.

(29) Conradie, M. M.; Conradie, J.; Gosh, A. A DFT overview of high-valent iron, cobalt and nickel tetraamidomacrocyclic ligand (TAML) complexes: The end of innocence? *J. Inorg. Biochem.* **2006**, *100*, 620−626.

(30) Saavedra Díaz, R. O.; Le Lagedec, R.; Shen, L. Q.; Ryabov, A. D. In search for chelating TAMLs (*t*etra*a*mido *m*acrocyclic *l*igands) with peripheral bidentate donor centers: a cobalt(III) complex of the 3,3′-(2,2′-bipyridindiyl)-tailed TAML. *J. Coord. Chem.* **2014**, *67*, 3909−3919.

(31) Ramidi, P.; Sullivan, S. Z.; Gartia, Y.; Munshi, P.; Griffin, W. O.; Darsey, J. A.; Biswas, A.; Shaikh, A. U.; Ghosh, A. Catalytic Cyclic Carbonate Synthesis Using Epoxide and Carbon Dioxide: Combined Catalytic Effect of Both Cation and Anion of an Ionic $Cr^{V}(O)$ Amido Macrocyclic Complex. *Ind. Eng. Chem. Res.* **2011**, *50*, 7800−7807.

(32) (a) Evans, D. F. The determination of the paramagnetic susceptibility of substances in solution by nuclear magnetic resonance. *J. Chem. Soc.* **1959**, 2003−2005. (b) Deutsch, J. L.; Poling, S. M. The determination of paramagnetic susceptibility by NMR: A physical chemistry experiment. *J. Chem. Educ.* **1969**, *46*, 167−168. (c) Piguet, C. Paramagnetic Susceptibility by NMR: The "Solvent Correction" Removed for Large Paramagnetic Molecules. *J. Chem. Educ.* **1997**, *74*, 815−816. (d) Sur, S. K. Measurement of magnetic susceptibility and magnetic moment of paramagnetic molecules in solution by high-field

DOI: 10.1021/jacs.9b11715
J. Am. Chem. Soc. 2020, 142, 552−563

fourier transform NMR spectroscopy. *J. Magn. Reson.* **1989**, *82*, 169−173. (e) Grant, D. H. Paramagnetic Susceptibility by NMR: The "Solvent Correction" Reexamined. *J. Chem. Educ.* **1995**, *72*, 39. (f) Hoppe, J. I. Effective magnetic moment. *J. Chem. Educ.* **1972**, *49*, 505. (g) Bain, G. A.; Berry, J. F. Diamagnetic Corrections and Pascal's Constants. *J. Chem. Educ.* **2008**, *85*, 532−536.

(33) Notably, a previous study (ref 23) on the electrochemical behavior of Na[Co^{III}($TAML^{red}$)] in MeCN displayed only one reversible oxidation event, whereas the second oxidation was found to be irreversible.

(34) Mak, S.-T.; Wong, W.-T.; Yam, V. W.-W.; Lai, T.-F.; Che, C.-M. Cobalt(III) alkyl complexes of 1,2-bis(2-pyridinecarboxamido)-benzene (H_2bpb) and 4,5-dichloro-1,2-bis(2-pyridinecarboxamido)-benzene (H_2bpc) and X-ray crystal structures of [Co(bpc)-($CH_2CH_2CMe = CH_2$)(H_2O)] and [Co(bpb)Et(H_2O)]. *J. Chem. Soc., Dalton Trans.* **1991**, 1915−1922.

(35) CASSCF calculations demonstrated that the absorption band at 623 nm is dominated by ligand-centered $\pi \rightarrow \pi^*$ and metal-to-ligand charge-transfer excitations. See the CASSCF section on [$\mathbf{Co^{III}(TAML^{sq})}$] for more details.

(36) (a) Connelly, N. G.; Geiger, W. E. Chemical Redox Agents for Organometallic Chemistry. *Chem. Rev.* **1996**, *96*, 877−910. (b) Boduszek, B.; Shine, H. J. Preparation of solid thianthrene cation radical tetrafluoroborate. *J. Org. Chem.* **1988**, *53*, 5142−4143.

(37) Lahanas, N.; Kucheryavy, P.; Lockard, J. V. Spectroscopic Evidence for Room Temperature Interaction of Molecular Oxygen with Cobalt Porphyrin Linker Sites within a Metal−Organic Framework. *Inorg. Chem.* **2016**, *55*, 10110−10113.

(38) Cramer, C. J. *Essentials of Computational Chemistry: Theories and Models*, 2nd ed; John Wiley & Sons Ltd: West Sussex, U.K., 2004; pp 205−210.

(39) (a) Angeli, C.; Cimiraglia, R.; Evangelisti, S.; Leininger, T.; Malrieu, J.-P. Introduction of *n*-electron valence states for multi-reference perturbation theory. *J. Chem. Phys.* **2001**, *114*, 10252−10264. (b) Angeli, C.; Cimiraglia, R.; Malrieu, J.-P. *N*-electron valence state perturbation theory: a fast implementation of the strongly contracted variant. *Chem. Phys. Lett.* **2001**, *350*, 297−305. (c) Angeli, C.; Cimiraglia, R.; Malrieu, J.-P. *n*-electron valence state perturbation theory: A spinless formulation and an efficient implementation of the strongly contracted and of the partially contracted variant. *J. Chem. Phys.* **2002**, *117*, 9138−9153.

(40) We attempted to rotate the uncorrelated orbital(s) back into the active space. However, this was unsuccessful. Moreover, the inclusion of orbitals with occupancy 2.00 in the active space should be avoided. Aravena, D.; Atanasov, M.; Chilkuri, V. G.; Guo, Y.; Jung, J.; Maganas, D.; Mondal, B.; Schapiro, I.; Sivalingam, K.; Ye, S.; Neese, F. *CASSCF Calculations in ORCA (4.2): A Tutorial Introduction*. https://orcaforum.kofo.mpg.de/app.php/dlext/?cat=4 (accessed Sept 17, 2019).

(41) CASSCF calculations demonstrated that no intense characteristic absorption bands are expected in the 400−850 nm region. See the CASSCF section on $[\mathbf{Co^{III}(TAML^{q})(NNs)_2}]^-$.

(42) An accurate simulation of the experimental spectrum proved to be challenging and was unsuccessful.

(43) Olivos Suarez, A. I.; Lyaskovskyy, V.; Reek, J. N. H.; van der Vlugt, J. I.; de Bruin, B. Nitrogen-Centred Ligand Radical Complexes; Classification, Spectroscopic Features, Reactivity and Catalytic Applications. *Angew. Chem., Int. Ed.* **2013**, *52*, 12510−12529.

(44) (a) Au, S.-M.; Fung, W.-H.; Cheng, M.-C.; Che, C.-M.; Peng, S.-M. Synthesis, characterisation and reactivity of novel bis(tosyl)-imidoruthenium(VI) porphyrin complexes; X-ray crystal structure of a tosylamidoruthenium(VI) porphyrin. *Chem. Commun.* **1997**, 1655−1656. (b) Au, S.-M.; Huang, J.-S.; Yu, W.-Y.; Fung, W.-H.; Che, C.-M. Aziridination of Alkenes and Amidation of Alkanes by Bis(tosylimido)-ruthenium(VI) Porphyrins. A Mechanistic Study. *J. Am. Chem. Soc.* **1999**, *121*, 9120−9132.

(45) See the SI for a description of CASSCF-calculated UV−vis excitation energies and EPR *g* values.

DOI: 10.1021/jacs.9b11715
J. Am. Chem. Soc. 2020, 142, 552−563